Quantum Entanglement and Bell Violation in Higgs Boson Decays

George Barker

Department of Physics, Keble Road, University of Oxford,
OX1 3RH, United Kingdom

Abstract

Quantum state tomography is used to reconstruct the bipartite spin density matrices of simulated diboson systems at energies achievable at the LHC. The Wigner-Weyl spin formalism is used to find the inverse mapping from the decay angular distributions to operators in the system's Hilbert space for $H \rightarrow WW$, $pp \rightarrow WZ$ and $H \rightarrow ZZ$. For the latter, a revised symmetric density matrix is proposed and tested. Measures of quantum entanglement and violation of Bell's inequalities for these systems are calculated, predicting all three systems showing evidence of non-classical correlations and both systems resulting from Higgs boson decays predicting incompatibility with local-realist theories. A method is presented for optimising such *Bell violation* through unitary transforms and determining its statistical significance. Analysis shows the *WW* system is expected to violate Bell's inequalities with certainty ~ 5.9σ, and similarly the *ZZ* system with ~ 1.0σ at an integrated luminosity of 300 fb^{-1}.

Section 1: Introduction

The technique of quantum state tomography enables the density matrix ρ of a quantum mechanical system to be determined from performing multiple measurements of similarly prepared states. With the knowledge of ρ, the expectation value of any measurement can be found from $\langle O \rangle = tr(\rho O)$ of its Hilbert-space operator O. Reconstructing ρ is therefore sufficient to investigate properties of the system, for example its quantum entanglement and conformity to Bell's inequalities [1].

Although traditionally quantum state tomography has been performed on low energy systems [2], more recently methods have been proposed by particle physicists to determine the spin density matrices of systems at energies accessible by the LHC. Quantum state tomography has been proposed before for pairs of spin-half fermionic systems at the LHC [3], where the method has been used to study the entanglement of simulated pairs of top and anti-top quarks. Recently, a more general method has been presented [4] for a system of one or more particles of spin $j \geq \frac{1}{2}$, enabling examination of the weak decays of massive bosons. The extension of quantum tomographic techniques from quantum information theory to particle physics is a compelling area for research due to the potential shortcomings of the standard model at high energies and the significant philosophical implications of Bell's inequalities. This experimental test of Bell's inequalities can therefore be used to investigate the differences between local realist and quantum theories.

This project uses these techniques to reconstruct the density matrices of simulated bipartite qutrit ($d = 2j+1 = 3$) systems, namely $H \rightarrow WW$, $pp \rightarrow WZ$ and $H \rightarrow ZZ$, and determines statistics indicating quantum entanglement and Bell violation. It then aims to extend these results to investigate the validity of the symmetrisation process in the $H \rightarrow ZZ$ case, as well as propose a technique to find the statistical significance of the Bell violation result. The relevant tests for Bell violation are then optimised through unitary transformations of the relevant operator, enabling a full description of the certainty of the test results. This report will initially cover the theoretical methodology behind reconstructing the spin density matrix from simulated decay data and introduce the operators of interest. The results of these techniques will then be presented and interpreted before presenting conclusions and indicating future work in this area.

Section 2: Methods

This section describes how quantum tomography has been performed in this project and the relevant theory behind the subsequent analysis, following the methods of [4].

2.1 Gell-Mann parameterisation of a bipartite spin density matrix

The density matrix represents the information we know about a partially known quantum system. It is defined as

$$\rho = \sum_i p_i |\psi_i\rangle\langle\psi_i| \tag{2.1}$$

where the p_i parameters are interpreted to be the classical probabilities of the system being in state $|\psi_i\rangle$. Conservation of probability $\sum_i p_i = 1$ dictates that ρ has unit trace, and consequently $\mathrm{tr}(\rho^n) \in [0,1]$ for integer n as the eigenvalues of ρ are also in this range, reducing the trace to a sum of powers of p_i that sum to unity. The Hilbert space $\mathcal{H}$ in which ρ is the density matrix of a single spin-j particle is $d = 2j+1$ dimensional. Viewing ρ as a Hermitian operator on this space, it must have $d^2 - 1$ real parameters due to the trace constraint. For a bipartite system, the density matrix acts on a Hilbert space $\mathcal{H} = \mathcal{H}_1 \otimes \mathcal{H}_2$ of dimension $d = (2j_1 + 1)(2j_2 + 1)$ and also has $d^2 - 1$ real parameters.

The eight 3-dimensional Gell-Mann (GM) matrices λ [7] are used to form a parameterisation of ρ:

$$\rho^{(9)} = \frac{1}{9} I_9 + \sum_{i=1}^{8} a_i \lambda_i \otimes \frac{1}{3} I_3 + \sum_{j=1}^{8} \frac{1}{3} I_3 \otimes b_j \lambda_j + \sum_{i=1}^{8} \sum_{j=1}^{8} c_{ij} \lambda_i \otimes \lambda_j \tag{2.2}$$

where the a_i and b_j are Bloch (polarisation) vectors for the individual particles, the c_{ij} represent the correlations between them and I_n is the identity matrix in n-dimensions. These form a useful basis as they are complete on the 9-dimensional Hilbert space of a pair of qutrits, non-redundant, symmetric and are equipped with the orthogonality relations

$$\mathrm{tr}(\lambda_i \lambda_j) = 2\delta_{ij},\ \ \mathrm{tr}(\lambda_i) = 0. \tag{2.3}$$

Using (2.3), the parameters of (2.2) can be extracted as expectation values of the Gell-Mann operators themselves, as described in Section 2.4. Finding these parameters is therefore equivalent to performing full quantum state tomography on the system.

2.2 Weyl-Wigner transformation

When analysing decay data, there are two options for finding information about the initial state of the system. Firstly, likelihood functions could be used to fit parameters from Monte Carlo simulations to the original operators. Secondly, an analytical inverse mapping (from angular decay data to operators in the Hilbert space) can be found. The second method has the advantage of being able to find analytical values for quantities calculable from the spin density matrix, in this case the Bell operator expectation value.

The Weyl-Wigner formalism [8] provides an invertible mapping between functions in the quantum phase space and operators in the Hilbert space. Here, we consider the phase space to be the angular decay distributions in $\mathcal{S}^2$ and the operators to be the spin density matrices operating in $\mathcal{H}$. Wigner Q symbols are used to map these operators $\mathcal{O} : \mathcal{H} \rightarrow \mathcal{H}$ to the functions on $\mathcal{S}^2$, and are defined as:

$$\Phi_{\mathcal{O}}^{Q}(\hat{\boldsymbol{n}}) = \langle \hat{\boldsymbol{n}} | \mathcal{O} | \hat{\boldsymbol{n}} \rangle \tag{2.4}$$

with $\hat{\boldsymbol{n}}$ a unit vector in $\mathbb{R}^3$. The inverse mapping is achieved by using Wigner P symbols, defined through the property

$$\mathcal{O} = \frac{2j+1}{4\pi} \int d\Omega_{\hat{n}} |\hat{\boldsymbol{n}}\rangle \Phi_{\mathcal{O}}^{P}(\hat{\boldsymbol{n}}) \langle \hat{\boldsymbol{n}}| \tag{2.5}$$

with the angular integral taken over all directions $\hat{\boldsymbol{n}}$. Using experimental data, we can find expectation values of these Wigner P functions to find the parameters required to form the density matrix in the GM basis (2.2). To find the Wigner P functions, the nature of the measurement must be considered, as the particles in the decay angular distributions considered couple differently to W and Z bosons.

2.3 Projective Measurements: W decay

To demonstrate the procedure, we first consider a single W boson (j= 1), with density matrix the first part of (2.2) and is fully characterized by the eight real a_i parameters:

$$\rho^{(3)} = \frac{1}{3} I_3 + \sum_{i=1}^{8} a_i \lambda_i \,. \tag{2.6}$$

The W boson is maximally parity violating, and only couples to left-chiral spin-half fermions and right-chiral spin-half anti-fermions [9]. As leptonic masses are much lower than the W's, we have equivalence between their helicity and chirality eigenstates, e.g. in the decay $W^+ \rightarrow \ell^+ \nu$, the ℓ^+ is produced in a +1 helicity state and the ν in a -1 helicity state, thus the spin of W^+ is measured to be +1 in the momentum direction of the anti-lepton. Measuring the decay directions of the leptons in the W rest frame therefore enables us to make a projective measurement of the boson's spin in that frame.

The probability of a $W^\pm$ emitting a lepton $\ell^\pm$ into a solid angle $d\Omega$ along the direction $\hat{\boldsymbol{n}}$ can be written as the expectation value of the spin-1 projector $\Pi_{\pm\hat{\boldsymbol{n}}}$ from the density matrix as

$$p\left(l^{\pm}(\hat{\boldsymbol{n}})\right) = \frac{3}{4\pi} \mathrm{tr}(\rho \Pi_{\pm\hat{\boldsymbol{n}}}) \tag{2.7}$$

where the normalisation fixes the integral of p over all $\hat{\boldsymbol{n}}$ to unity. The spin-1 projection operator is defined to pick out the states of W decay in that direction, for example $\Pi_{+\hat{\boldsymbol{n}}} = |+\rangle_{\hat{\boldsymbol{n}}} \langle +|_{\hat{\boldsymbol{n}}}$ explicitly picks out a ℓ^+ with helicity +1 in the $\hat{\boldsymbol{n}}$ direction alongside a ν with helicity -1 in the $-\hat{\boldsymbol{n}}$ direction. The $\Pi_{\pm\hat{\boldsymbol{n}}}$ projector can be found by rotating the states $|\pm\rangle_{\hat{\boldsymbol{z}}} \langle \pm|_{\hat{\boldsymbol{z}}}$, which have spin ±1 in the $\hat{\boldsymbol{z}}$ direction, about a polar angle θ and azimuthal angle ϕ. The form of this spin-1 projector can be found in Appendix 1.

Using the parameterisation (2.6) in (2.7), we can determine an analytical expression for the probability distribution in terms of the a_i parameters as

$$p\left(l^{\pm}(\hat{\boldsymbol{n}})\right) = \frac{3}{4\pi}\left(\frac{1}{3} + \sum_{i=1}^{8} a_i \Phi_i^{Q\pm}\right) \tag{2.8}$$

with

$$\Phi_i^{Q\pm} = tr(\lambda_i \Pi_{\pm\hat{\boldsymbol{n}}}) = \langle \pm\hat{\boldsymbol{n}} |\, \lambda_i \,| \pm\hat{\boldsymbol{n}} \rangle. \tag{2.9}$$

The first equality in (2.9) can be seen from the orthogonality relation (2.3) and rewriting with the second equality it is clear the $\Phi_i^{Q\pm}$ symbols are Wigner Q functions in the terms of (2.4). These Wigner Q symbols are functions of θ and ϕ only and are written out in completeness in Appendix 2.

To determine the corresponding Wigner P values, the orthogonality relations (2.3) are rewritten in terms of Wigner P (using (2.5), with the operator $O = \lambda_j$) and Q symbols:

$$\begin{aligned} 2\delta_{ij} &= \mathrm{tr}(\lambda_i \lambda_j) \\ &= \mathrm{tr}\left(\lambda_i \, \frac{3}{4\pi} \int d\Omega_{\hat{n}} \; |\hat{\boldsymbol{n}}\rangle \, \Phi_j^{P+}(\hat{\boldsymbol{n}}) \, \langle \hat{\boldsymbol{n}}| \right) \\ 2\delta_{ij} &= \frac{3}{4\pi} \int d\Omega_{\hat{\boldsymbol{n}}} \, \Phi_j^{P+}(\hat{\boldsymbol{n}}) \, \Phi_i^{Q+}(\hat{\boldsymbol{n}}) \end{aligned} \tag{2.10}$$

∴

where the trace has been taken as $\mathrm{tr}(A) = \sum_\alpha |\alpha\rangle\, A\, \langle\alpha|$, alongside using the identity relation $I = \sum_\alpha |\alpha\rangle\langle\alpha|$ and the definition of Q symbols (2.4). As the Gell-Mann matrices are traceless, the integral of each P symbol over all $\hat{\boldsymbol{n}}$ must also vanish. The eight Wigner P functions that satisfy these criteria can therefore be calculated from the known Wigner Q symbols:

$$\Phi_i^{P\pm}(\hat{\boldsymbol{n}}) = [M^{-1}]_{ij}\ \Phi_j^{Q\pm}(\hat{\boldsymbol{n}}) \tag{2.11}$$

with the relationship (2.10) satisfied when M is calculated from the inner product:

$$\begin{aligned} M_{ij} &= \frac{d}{2}\langle\, \Phi_i^{Q\pm}\ \Phi_j^{Q\pm}\rangle \\ &= \frac{1}{2}\frac{3}{4\pi}\int d\Omega_{\hat{n}}\ \Phi_i^{Q\pm}(\hat{\boldsymbol{n}})\ \Phi_j^{Q\pm}(\hat{\boldsymbol{n}}) \end{aligned} \tag{2.12}$$

Inverting the matrix M, we can therefore find the full set of Wigner P symbols, which are given in Appendix 3.

Using (2.10) and the vanishing integral of each Wigner P function, along with (2.8), we finally arrive at the expression

$$a_i = \frac{1}{2}\int d\Omega_{\hat{n}}\ p\left(l^\pm(\hat{\boldsymbol{n}})\right)\ \Phi_i^{P\pm}(\hat{\boldsymbol{n}}) \tag{2.13}$$

which we can use to find the eight real parameters of $\rho^{(3)}$ (2.6) from the experimental average

$$\widehat{a_i} = \frac{1}{2}\langle\, \Phi_i^{P\pm}(\hat{\boldsymbol{n}})\rangle. \tag{2.14}$$

2.4 General non-projective (Z boson) bipartite decays

When we no longer have projective decays, the process in Section 2.1 must be generalised. Z bosons, unlike W bosons, couple to both left and right chiral fermions with coupling [9] given by

$$-\frac{i g_W}{\cos\theta W}\gamma^\mu(c_V - c_A\gamma^5) \tag{2.15}$$

where the vector and axial couplings $c_V = c_R + c_L$ and $c_A = c_L - c_A$ can be written in terms of right and left chiral couplings respectively, with g_W and θW the weak coupling and mixing angle. Following the procedure in [4], we can then define measurement operators F_l similarly to the projectors $\Pi_{\pm\hat{\boldsymbol{n}}}$, but for non-projective decays, in terms of the decay rate from an initial spin-m state i_m to a final state f as

$$[F_l]_{mm'} = \frac{\Gamma(i_m \to f)}{\Sigma_m \Gamma(i_m \to f)}\delta_{mm'}. \tag{2.16}$$

In analogy with the projectors, we can then define versions of F_l that are rotated from the frame aligned with the daughter momentum direction $F_{l,\hat{\boldsymbol{n}}} = U(\theta,\phi)\, F_l\, U^\dagger(\theta,\phi)$, and can therefore define generalised versions of (2.7) and (2.9):

$$p\left(l^\pm(\hat{\boldsymbol{n}})\right) = \tfrac{3}{4\pi} tr\left(\rho\, F_{l,\hat{\boldsymbol{n}}}\right), \qquad \widetilde{\Phi}_i^Q = tr\left(\lambda_i F_{l,\hat{\boldsymbol{n}}}\right) \tag{2.17a}$$

where the tilde denotes the generalised Wigner Q functions. Following the same procedure as before, we can then write $\widehat{a_i} = \frac{1}{2}\langle\, \widetilde{\Phi}_i^P\,\rangle$. Using (2.15), the non-projective measurement operators $F_{l,\hat{\boldsymbol{n}}}$ can be found and used in (2.17a) to find the generalised Wigner Q functions for Z → ℓℓ decay. It can be shown [4] that these can be written in terms of the standard Wigner Q functions as

$$\widetilde{\Phi}_{F_Z,j}^Q = \frac{1}{|C_R|^2 + |C_L|^2}\left(|C_R|^2\Phi_j^{Q+} + |C_L|^2\Phi_j^{Q-}\right). \tag{2.17b}$$

The generalised Wigner P functions can then be found from these, replacing $\Phi_i^{Q\pm}$ with $\widetilde{\Phi}^{Q}_{F_z,i}$ in (2.11) and (2.12). These can also be written in terms of the projective Wigner P values,

$$\widetilde{\Phi}^{P}_{F_z,j} = A_{jk}\,\Phi_j^{P+} \tag{2.18}$$

with the matrix A given in Appendix 4.

In a bipartite decay, the directions $\hat{\boldsymbol{n}}_1$ and $\hat{\boldsymbol{n}}_2$ of the emitted leptons are measured. The bipartite decay probability, a generalisation of (2.17a),

$$p(\hat{\boldsymbol{n}}_1,\hat{\boldsymbol{n}}_2) = \left(\frac{3}{4\pi}\right)^2 \mathrm{tr}\left(\rho\ F_{l,\hat{\boldsymbol{n}}_1}{}^{(A)} \otimes F_{l,\hat{\boldsymbol{n}}_2}{}^{(B)}\right) \tag{2.19a}$$

captures the decay of a spin-1 boson A decaying with a lepton in $\hat{\boldsymbol{n}}_1$ in the same system as the decay of another spin-1 boson B decaying to a lepton along $\hat{\boldsymbol{n}}_2$. The a_i parameters of (2.3) can therefore be extracted as $\hat{a}_i = \frac{1}{2}\langle\ \widetilde{\Phi}_i^{P}(\hat{\boldsymbol{n}}_1)\rangle$, where the average is over Wigner P functions generalised for the decay of boson A, and similarly the b_i parameters from $\hat{b}_i = \frac{1}{2}\langle\ \widetilde{\Phi}_i^{P}(\hat{\boldsymbol{n}}_2)\rangle$, where the functions represent the decay of boson B. The c_{ij} parameters can be extracted as a double integral over (2.19a), and can be extracted experimentally from the averages

$$\hat{c}_{ij} = \left(\frac{1}{2}\right)^2 \langle \widetilde{\Phi}^{P}{}_{F_l^{(A)},i}\,(\hat{\boldsymbol{n}}_1)\ \widetilde{\Phi}^{P}{}_{F_l^{(B)},j}(\hat{\boldsymbol{n}}_2)\rangle. \tag{2.19b}$$

2.5 Computational procedure for reconstructing ρ

Using data from Monte Carlo simulations generated using MadGraph v2.9.2 software [6], angular distributions of emitted leptons from bosonic decays are analysed. The 10^6 events for each file were generated to leading order at a proton-proton centre-of-mass energy of 13TeV employing the Higgs effective-field model. The processes of interest are shown in Figure 1.

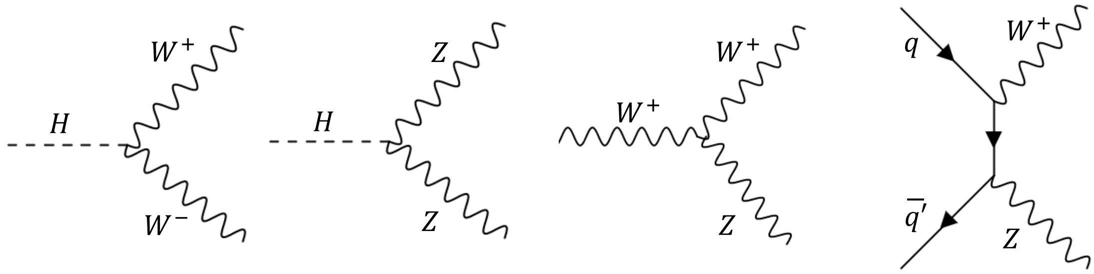

Figure 1: Di-bosonic systems of interest. In each case, the W bosons decay *projectively* and semi-leptonically, and the Z bosons decay *non-projectively* to lepton anti-lepton pairs.

During this project, original Python scripts were created to perform the tomography of such systems, as well as full analysis of the results. For Z decays, a minimum dilepton invariant mass cut of 20 GeV was implemented to reduce the background. The procedure reconstructs the directions of the decay product in their parent's rest frame in the basis described in [10], where the direction of the W^+ (or one of the Z bosons in $H \rightarrow ZZ$, see below) in the diboson centre-of-mass frame is labelled $\hat{\boldsymbol{k}}$. In this frame, the direction $\hat{\boldsymbol{p}}$ of one of the incoming beams is also found, enabling the formation of the orthonormal basis,

$$\hat{\boldsymbol{k}}, \quad \hat{\boldsymbol{r}} = \frac{1}{r}(\hat{\boldsymbol{p}} - y\,\hat{\boldsymbol{k}}), \quad \hat{\boldsymbol{n}} = \frac{1}{r}(\hat{\boldsymbol{p}} \times \hat{\boldsymbol{k}}) \tag{2.20}$$

where $y = \hat{\boldsymbol{p}} \cdot \hat{\boldsymbol{k}}$ and $r = \sqrt{1-y^2}$. Two different coordinate systems can then be found with boosts into the rest frame of a single boson (along $\hat{\boldsymbol{k}}$ or $-\hat{\boldsymbol{k}}$). These boosts leave $\hat{\boldsymbol{r}}$ and $\hat{\boldsymbol{n}}$ unaffected but requires re-normalisation of $\hat{\boldsymbol{k}}$. The purpose of the Python script is to find the directions of the emitted leptons in these bases, and to use these to find the required averages of the relevant Wigner P functions.

An added complexity in the $H \rightarrow ZZ$ case is that the decay parents are identical bosons. The quantum state, and therefore spin density matrix, must therefore be symmetric in swapping their labels. In this case it is proposed [4] that

$$\widehat{a_i} = \widehat{b_i} = \frac{1}{4}\langle \tilde{\Phi}^P{}_{F_Z(A),i}\,(\hat{\boldsymbol{n}}_1) + \tilde{\Phi}^P{}_{F_Z(B),i}\,(\hat{\boldsymbol{n}}_2)\rangle \tag{2.21}$$

$$\widehat{c_{ij}} = \frac{1}{8}\langle \tilde{\Phi}^P{}_{F_Z(A),i}\,(\hat{\boldsymbol{n}}_1)\tilde{\Phi}^P{}_{F_Z(B),j}\,(\hat{\boldsymbol{n}}_2) + \tilde{\Phi}^P{}_{F_Z(A),j}\,(\hat{\boldsymbol{n}}_1)\tilde{\Phi}^P{}_{F_Z(B),i}\,(\hat{\boldsymbol{n}}_2)\rangle. \tag{2.22}$$

As discussed in Section 3, these expressions give unphysical expectation for both operators defined in Section 2.6. A further factor of ½ has been proposed for the matrix, which results in a density matrix that does not have this issue.

2.6 Quantum Measurements from ρ

A bipartite quantum state is said to be entangled when a measurement of one of the particles affects a measurement of the other. This is equivalent to saying that the state cannot be written as the direct product of the subsystems' states. Measuring the entanglement of the d = 3x3 system in question is not possible analytically, however a concurrence value greater than zero has been shown [11] to only occur in entangled systems. In these bipartite systems, entanglement can be shown by evaluating a calculable lower bound of the concurrence of the system. One such bound on the square of the concurrence [12] denoted $c_{MB}{}^2$ can be expressed [4] in terms of the Gell-Mann parameters of ρ as

$$c_{MB}^2 = -\frac{4}{9} - \frac{2}{3}\sum_{i=1}^{8} a_i^2 - \frac{2}{3}\sum_{j=1}^{8} b_j^2 + 8\sum_{i,j=1}^{8} c_{ij}^2. \tag{2.23}$$

A value of $c_{MB}^2 > 0$ therefore implies an entangled system; $c_{MB}^2 \leq 0$ gives an inconclusive result.

Local realist theories impose that information cannot travel faster than the speed of light, and that properties of systems are real and independent of the manner of their measurement. Bell's inequalities [1] are a set of inequalities that such local realist theories must obey by requiring the marginal PDFs for measurements of each subsystem to be non-negative.

For a system of a pair of qutrits, the CGLMP inequality [13] has been shown to be the optimal test of conformity of a system to Bell's inequalities. Within quantum mechanics, we can represent this test with *Bell operators* $\mathcal{B}$, where local-realist theories must abide by the inequality

$$\langle \mathcal{B} \rangle = \mathrm{tr}(\rho\mathcal{B}) \leq 2. \tag{2.24}$$

A quantum operator for the CGLMP test suited to bipartite qutrit systems (2.25) is defined in [10] and can be written in terms of the $j=1$ spin operators and Gell-Mann matrices, given in Appendices 5 and 6 respectively.

$$B_{CGLMP} = -\frac{2}{\sqrt{3}}\left(S_x \otimes S_x + S_y \otimes S_y\right) + \lambda_4 \otimes \lambda_4 + \lambda_5 \otimes \lambda_5 \tag{2.25}$$

The largest value of $\langle B_{CGLMP}\rangle$ is ~2.8729 when the state is maximally entangled [13], and ~2.9149 when not [14]. This CGLMP operator is a function of spin operators in the xy plane only, with this freedom of choice of measurements corresponding to the unitary transformations

$$\langle B_{CGLMP}\rangle_{max} = max\left(tr\left((U \otimes V)^\dagger \cdot B_{CGLMP} \cdot (U \otimes V)\right)\right. \tag{2.26}$$

of (2.25) still representing a valid Bell operator [5]. Here, $U, V \in SU(3)$ are independent and generated by the Gell-Mann matrices, giving sixteen real parameters to optimise over. This optimisation is performed in Section 3.3.

Section 3: Results

In this section the results of the quantum tomography described in Section 2 and the subsequent analysis are presented.

3.1 Reconstructed spin density matrices

Using the procedure from Section 2, the spin density matrices are reconstructed in the Gell-Mann basis for $H \rightarrow WW$, $pp \rightarrow WZ$ and $H \rightarrow ZZ$, with the results shown in Figure 2. The density matrix is also shown for the non-relativistic, narrow-width j=1 ⊗ j=1 singlet state

$$|\psi_s\rangle = \frac{1}{\sqrt{3}}(|+\rangle|-\rangle - |0\rangle|0\rangle + |-\rangle|+\rangle). \tag{3.1}$$

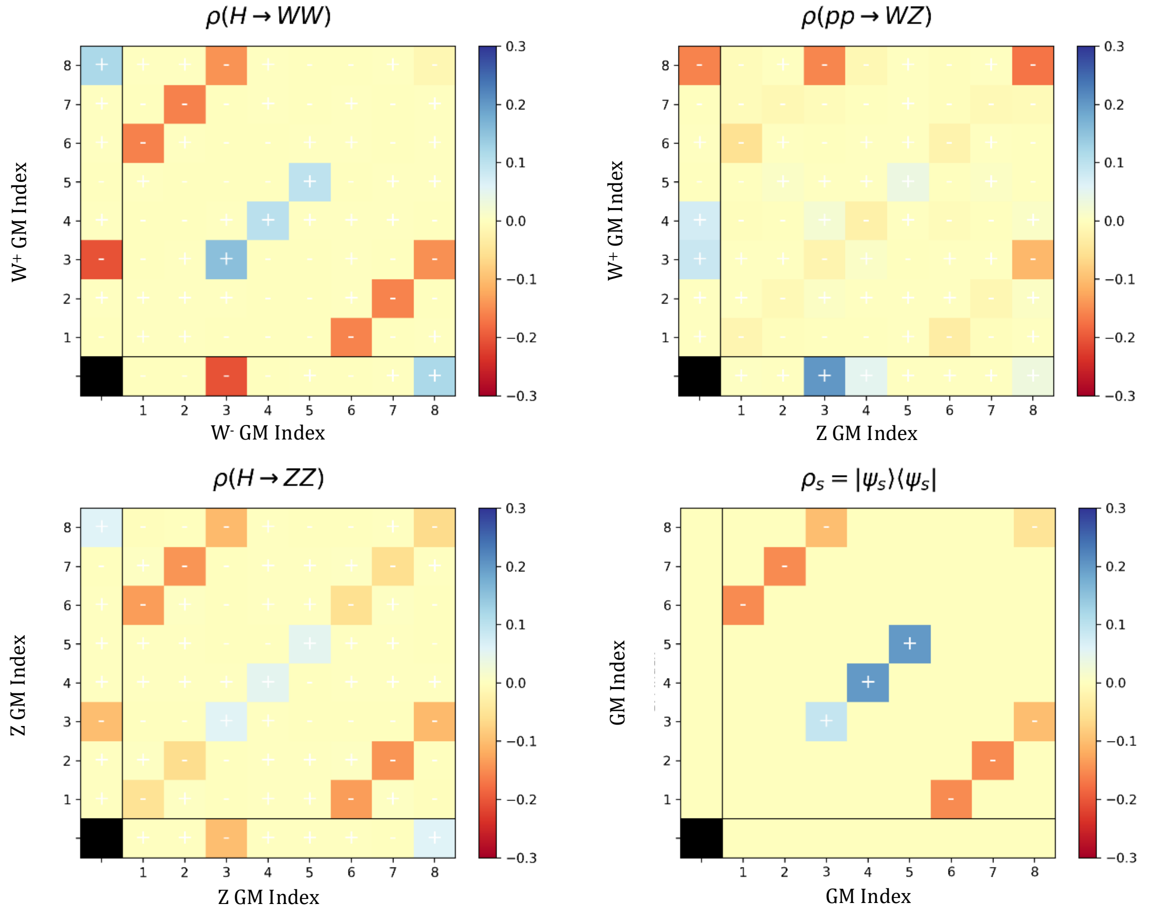

Figure 2: Reconstructed Gell-Mann parameters from the decays in Figure 1. The a_i and b_j values are shown in the 0^{th} row and column respectively, with c_{ij} the remaining *8x8* matrix. The (0,0) value is meaningless. The ZZ density matrix is exactly half that of the parameters found in (2.21) and (2.22).

In Figure 2, the non-zero values corresponding to the c_{ij} GM parameters indicate correlations between the two bosons. We can also observe that the $H \rightarrow WW$ decay shares many similarities with the spin singlet state $|\psi_s\rangle$, a state to which it reduces to in the narrow-width and non-relativistic limit. The Higgs decay does, however, vary from the singlet state, mainly in the 3rd and 8th GM index. The square of the concurrence is then found for each ρ, as described in Section 2.6, and is tabulated in Table 1. All systems have a value for the lower bound of the concurrence squared c_{MB}^2 greater than zero, and so we conclude there is evidence for quantum entanglement in these systems.

Table 1 again includes an extra factor of ½ in the symmetrised spin density matrix. Before adding this to (2.21) and (2.22), c_{MB}^2 = 3.4380 which is higher than the maximally entangled singlet state for a pair of qutrits and therefore not possible.

Bipartite Quantum System	c_{MB}^2
$H \rightarrow \boldsymbol{W^+W^-} \rightarrow \ell^+ \nu \, \ell^- \nu$	0.9733
$pp \rightarrow \boldsymbol{W^+Z} \rightarrow e^+ \nu_e \, \mu^+ \mu^-$	0.0980
$H \rightarrow \boldsymbol{ZZ} \rightarrow \mu^+ \mu^- e^+ e^-$	0.5262
$\lvert \boldsymbol{\psi_s} \rangle$	$^4/_3$

Table 1: Lower bound on concurrence c_{MB}^2 for the spin density matrices from quantum tomography of the simulated bipartite systems. The system for which the density matrix is formed is in **bold**.

3.2 Bell Operator Expectation Values

The CGLMP test is performed on each of the million events by finding the expectation values of (2.25) and (2.26) for each event's contribution to the spin density matrix. The distributions are shown in Figure 3, with the expectation value of the mean spin density matrix (as shown in Figure 2) in Table 2.

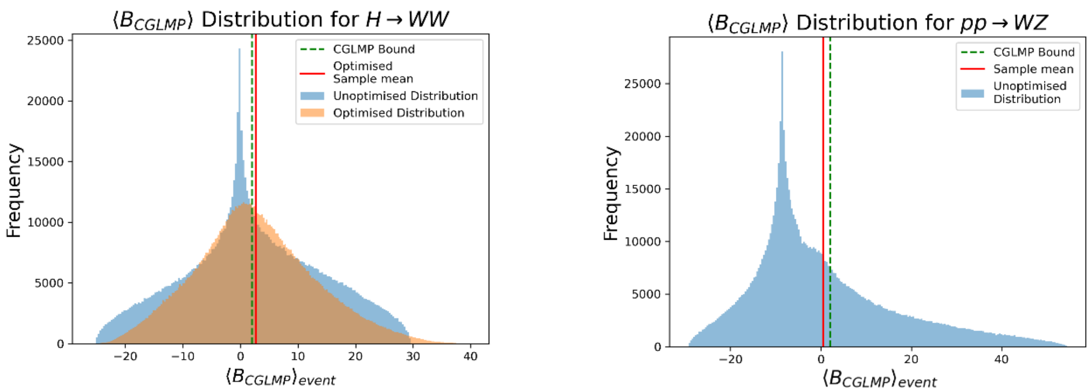

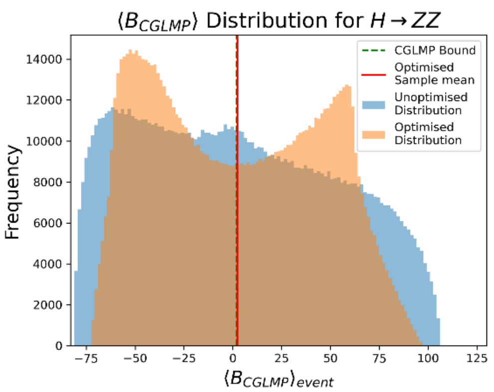

Bipartite Quantum System	$\langle \boldsymbol{B_{CGLMP}} \rangle$
$H \rightarrow \boldsymbol{W^+W^-} \rightarrow \ell^+\nu\ell^-\nu$	2.2571
$pp \rightarrow \boldsymbol{W^+Z} \rightarrow e^+\nu_e\mu^+\mu$	0.4489
$H \rightarrow \boldsymbol{ZZ} \rightarrow \mu^+\mu^-e^+e^-$	2.2023

Table 2: Mean expectation value of the unoptimised (2.25) CGLMP operator.

Figure 3: Distributions of $\langle B_{CGLMP} \rangle$ in the qutrit-pair quantum states. The CGLMP bound of 2 is also plotted alongside the sample mean; their order indicative of conformity to local-realist theories. For the Bell-violating processes, the distribution for the optimised Bell operator (2.26) is also shown.

Since these are clearly non-Gaussian distributions, we cannot view the rms of these as the uncertainty in the mean. Instead, $M = 10^4$ random samples of $\langle B_{CGLMP} \rangle$ have been taken (with M chosen to produce a suitably fine-grained histogram) from the 10^6 data points. Each random sample was of size

$$N_i = L\,\sigma_i \tag{3.2}$$

where L is the integrated luminosity of the LHC (taken as 300 fb^{-1}) and σ_i is the total cross-section for the process i, taken from MadGraph. The mean from these samples can then be plotted and fitted to a

Gaussian as shown in Figure 4. This process is therefore equivalent to running the LHC at this luminosity M times and finding the standard deviation in the distribution of the experimentally measured mean $\langle B_{CGLMP} \rangle$, thus giving us a measure of uncertainty in the results presented in Table 2.

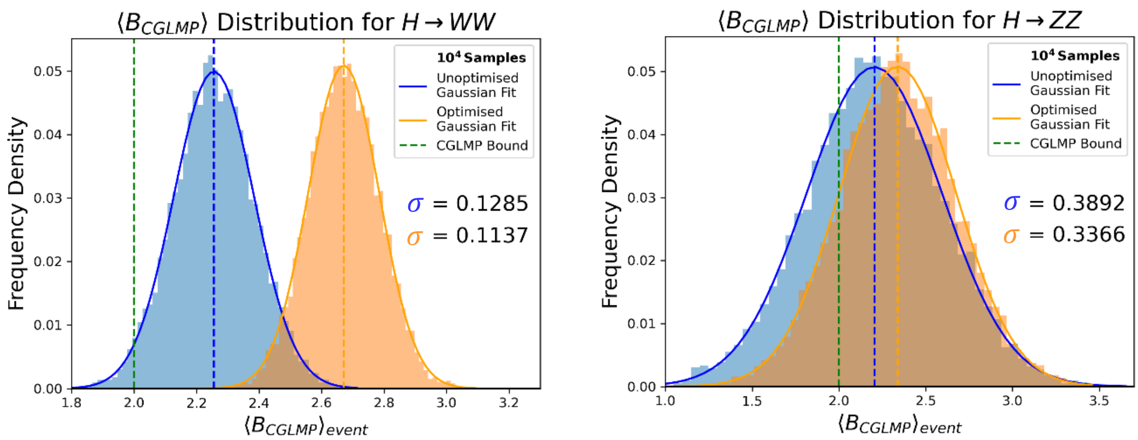

Figure 4: Distribution of random sample means from $\langle B_{CGLMP} \rangle$ event distribution for the two Bell violating events. The equivalent graphic for $pp \rightarrow WZ$ can be seen in Appendix 7. The distribution for the optimised CGLMP operator (2.26) is also shown in orange.

The mean and σ of this fit are recorded so the number of standard deviations of this mean above the CGLMP limit of 2 can be found as a measure of uncertainty. Using this method, before optimisation, we can conclude that the WW pair from the process $H \rightarrow WW$ violate Bell's inequalities with certainty of ~ 2.0σ and that the ZZ pair from $H \rightarrow ZZ$ violate Bell's inequalities with a certainty ~ 0.52σ.

3.3 Unitary Transforms of CGLMP Bell Operator

A suitable parameterised analytical expression for (2.26) could not (using *Mathematica*) be found. Instead, numerical optimisation was employed, where an implementation [15] of the *Nelder-Mead* algorithm for the SciPy library was found to perform better than other suitable algorithms. To cover the full 4π range of possibilities ($exp(i\, a_i\, (\lambda_i/2))$ is invariant under $a_i \rightarrow a_i + 4\pi$ for any Gell-Mann matrix λ_i) for each of the sixteen real parameters, optimisation is performed for integer combination of bounds in the range of -7 to +7 and the resulting maximum used. Equation (2.26) reverts to (2.25) when the a_i identically vanish. The results of these optimisations are shown in Table 3, with the corresponding values of U and V given in Appendix 8.

Bipartite Quantum System	$\boldsymbol{max(\langle B_{CGLMP} \rangle)}$	$\boldsymbol{\frac{max(\langle B_{CGLMP} \rangle) - 2}{\sigma}}$
$H \rightarrow W^+W^- \rightarrow \ell^+\nu\ell^-\nu$	2.6710	5.9032
$H \rightarrow ZZ \rightarrow \mu^+\mu^-e^+e^-$	2.3382	1.0050

Table 3: Results from optimised CGLMP Bell operator. The statistical significance of the violation is shown in the third column, with the relevant values taken from Figure 4.

Section 4: Interpretation

4.1 Spin density matrices

All values for the square of concurrence lower bound and $\langle B_{CGLMP} \rangle$ for the spin density matrices shown in Figure 2 are within theoretical physical bounds (see Section 2.6). These results are similar to those previously presented in [4]. The small differences in the c_{MB}^2 (~ 3% higher for WW case) are due to the simulated files analysed here having fewer selection cuts. When the Python scripts for this project were run for the same datasets as [4], identical results were obtained. This implies that the selection cuts were favouring the less entangled, higher energy events.

Particular attention has been given to the symmetrisation of the $H \rightarrow ZZ$ case. Using the parameters (2.21) and (2.22), defined in [4], physical results for the concurrence and $\langle B_{CGLMP} \rangle$ are not achieved, giving c_{MB}^2 = 3.4380, higher than the maximally entangled state (Table 1) and (unoptimised) $\langle B_{CGLMP} \rangle$ = 4.4045, higher than the upper bound given in [4]. This is also done in other works such as [5] without explicit justification. Multiplying all the Gell-Mann parameters by ½, physical results are obtained and presented in Section 3. It has also been verified that the relationship $\mathrm{tr}(\rho^n) \in [0,1]$ is only valid with this additional factor. The theoretical reasoning behind this additional factor is yet to be presented, although could be representing the fact that a symmetric state has half the number of states available in its Fock space compared to an analogous asymmetric state.

<u>4.2 CGLMP Bell tests</u>

The mean $\langle B_{CGLMP} \rangle$ values presented in Table 2 are again similar to those presented in [4] (with the exception of the *ZZ* case, see above). In the data with selection cuts, $\langle B_{CGLMP} \rangle$ = 2.2480 for the WW system and $\langle B_{CGLMP} \rangle$ = 0.4969 for the WZ system. Removing the cuts (as in Section 3) therefore changes this value by up to 5%, however does not change the conclusions of whether either system adheres to Bell's inequalities. The distributions in Figure 3 of the Bell operator over the entire data set appear unusual, with a large variation in the CGLMP Bell expectation value. These distributions seem to have no common features. In all cases, the difference between the mean and the local-realist limit appears to be small in comparison to this variation, indicating a need for a more careful statistical treatment. This is provided in Figure 4, where Gaussian distributions are shown with a much lower variation. We can therefore say that the WW system violates Bell's inequalities with more certainty than the *ZZ* system.

<u>4.3 Optimisation of CGLMP Bell test</u>

We observe the optimisation in Table 3 has produced a significant increase in the certainty of the expected Bell violation in both Higgs decays, with the optimisation increasing $\langle B_{CGLMP} \rangle$ by 18% and by 6% for the WW and ZZ systems respectively. The *U* and *V* matrices found in this procedure all demonstrate unitarity to $\mathcal{O}(10^{-8})$, indicating the validity of these results. In Figure 3, we note the effect optimisation of the CGLMP operator has had on the distributions, with few obvious similarities to the unoptimised equivalents. In both cases, the optimisation has the effect of reducing the standard deviation of the distributions as seen in Figure 4. This project therefore builds on the work of [5] where this method has been shown to increase $\langle B_{CGLMP} \rangle$ in the cases of $H \rightarrow WW^*$ and $H \rightarrow ZZ^*$, with (*) denoting an off-shell state. It has also shown the validity of using this method when optimising over the mean density matrix for the entire ensemble of decays. It has been noted [10], that small ($\mathcal{O}(10)$) ensembles may align the density matrix with statistical fluctuations causing $\langle B_{CGLMP} \rangle$ to increase further. The ensembles here were of order 10^6, so such effects are ignored.

Section 5: Conclusion

This project has used quantum state tomography to find the bipartite spin density matrices of bosonic systems formed at the LHC. Using simulated data, it has found evidence of quantum entanglement in such systems and investigated whether the diboson pair is reconcilable with local-realist theories by testing Bell's inequalities. This project has shown that the decays $H \rightarrow WW$ and $H \rightarrow ZZ$ violate these inequalities using the CGLMP test, and has found the unitary transforms that maximise this violation. A procedure for finding the statistical significance of such violation has also been presented, giving these results ~ 5.9σ and ~ 1.0σ significance for the simulated WW and ZZ systems respectively.

These results aid the possibility of experimentally measuring quantum entanglement and violation of Bell's inequalities in future experiments at the LHC, increasing our knowledge of Higgs decays and conformity of high-energy physics to local-realist theories. Attempting to reproduce the results presented in this report with experimental data would therefore be an interesting area for future research. Finding justification for the unfamiliar distributions in Figure 3 presents an interesting theoretical problem as they may be a result of unconsidered physical effects. The object-orientated Python scripts created during this project can also be used for any similar quantum system, and therefore could be used to find more evidence for violation of Bell's inequalities in particle physics.

Appendix 1: $j = 1$ projection operator

The projection operator $\Pi_{\pm\hat{\boldsymbol{n}}}$ required to find the angular decay distribution of a projective decay in the sense of

$$p\left(l^{\pm}(\hat{\boldsymbol{n}})\right) = \frac{3}{4\pi} tr(\rho \Pi_{\pm\hat{\boldsymbol{n}}})$$

can be found by rotating the z-polarized states with unitary rotations $U(\theta, \phi) \in \mathrm{SU}(2)$:

$$\Pi_{\pm\hat{\boldsymbol{n}}} = U(\theta,\phi)|\pm\rangle_{\hat{z}}\langle\pm|_{\hat{z}}\, U^{\dagger}(\theta,\phi)$$

$$\Pi_{+\hat{\boldsymbol{n}}} = \begin{pmatrix} \cos^4\frac{\theta}{2} & \frac{1}{2\sqrt{2}}e^{-i\phi}\sin\theta(1+\cos\theta) & \frac{1}{4}e^{-2i\phi}\sin^2\theta \\ \frac{1}{2\sqrt{2}}e^{i\phi}\sin\theta(1+\cos\theta) & \frac{1}{2}\sin^2\theta & \frac{1}{2\sqrt{2}}e^{-i\phi}\sin\theta(1-\cos\theta) \\ \frac{1}{4}e^{2i\phi}\sin^2\theta & \frac{1}{2\sqrt{2}}e^{i\phi}\sin\theta(1-\cos\theta) & \sin^4\frac{\theta}{2} \end{pmatrix}$$

With the equivalent $\Pi_{-\hat{\boldsymbol{n}}}$ version found from $\theta \rightarrow \pi - \theta$ and $\phi \rightarrow \phi + \pi$.

Appendix 2: Projective Wigner Q symbols for W decay

The eight functions in (2.8) have been calculated [4] from the 8 Gell-Mann matrices as follows:

$$\begin{aligned}
\Phi_1^{Q\pm} &= \tfrac{1}{\sqrt{2}}\sin\theta(\cos\theta\pm1)\cos\phi & \Phi_5^{Q\pm} &= \tfrac{1}{2}\sin^2\theta\sin2\phi \\
\Phi_2^{Q\pm} &= \tfrac{1}{\sqrt{2}}\sin\theta(\cos\theta\pm1)\sin\phi & \Phi_6^{Q\pm} &= \tfrac{1}{\sqrt{2}}\sin\theta(-\cos\theta\pm1)\cos\phi \\
\Phi_3^{Q\pm} &= \tfrac{1}{8}(\pm4\cos\theta+3\cos2\theta+1) & \Phi_7^{Q\pm} &= \tfrac{1}{\sqrt{2}}\sin\theta(-\cos\theta\pm1)\sin\phi \\
\Phi_4^{Q\pm} &= \tfrac{1}{2}\sin^2\theta\cos2\phi & \Phi_8^{Q\pm} &= \tfrac{1}{8\sqrt{3}}(\pm12\cos\theta-3\cos2\theta-1)\,.
\end{aligned}$$

Appendix 3: Projective Wigner P symbols for W decay

The eight functions in (2.11) have been calculated [4] from the 8 Gell-Mann matrices as follows:

$$\begin{aligned}
\Phi_1^{P\pm} &= \sqrt{2}(5\cos\theta\pm1)\sin\theta\cos\phi & \Phi_5^{P\pm} &= 5\sin^2\theta\sin2\phi \\
\Phi_2^{P\pm} &= \sqrt{2}(5\cos\theta\pm1)\sin\theta\sin\phi & \Phi_6^{P\pm} &= \sqrt{2}(\pm1-5\cos\theta)\sin\theta\cos\phi \\
\Phi_3^{P\pm} &= \tfrac{1}{4}(\pm4\cos\theta+15\cos2\theta+5) & \Phi_7^{P\pm} &= \sqrt{2}(\pm1-5\cos\theta)\sin\theta\sin\phi \\
\Phi_4^{P\pm} &= 5\sin^2\theta\cos2\phi & \Phi_8^{P\pm} &= \tfrac{1}{4\sqrt{3}}(\pm12\cos\theta-15\cos2\theta-5)\,.
\end{aligned}$$

Appendix 4: Generalised Wigner P symbols for Z → ℓℓ decay

These functions of θ and ϕ can be found [4] from (2.18), where the matrix A is given by:

$$A = \frac{1}{|c_R|^2-|c_L|^2}\begin{pmatrix}
|c_R|^2 & 0 & 0 & 0 & 0 & |c_L|^2 & 0 & 0 \\
0 & |c_R|^2 & 0 & 0 & 0 & 0 & |c_L|^2 & 0 \\
0 & 0 & |c_R|^2-\frac{1}{2}|c_L|^2 & 0 & 0 & 0 & 0 & \frac{\sqrt{3}}{2}|c_L|^2 \\
0 & 0 & 0 & |c_R|^2-|c_L|^2 & 0 & 0 & 0 & 0 \\
0 & 0 & 0 & 0 & |c_R|^2-|c_L|^2 & 0 & 0 & 0 \\
|c_L|^2 & 0 & 0 & 0 & 0 & |c_R|^2 & 0 & 0 \\
0 & |c_L|^2 & 0 & 0 & 0 & 0 & |c_R|^2 & 0 \\
0 & 0 & \frac{\sqrt{3}}{2}|c_L|^2 & 0 & 0 & 0 & 0 & \frac{1}{2}|c_L|^2+|c_R|^2
\end{pmatrix}$$

Where $c_R = 0.233$ and $c_L = -0.273$ are the right- and left- handed chiral couplings of a Z boson to a lepton.

Appendix 5: j=1 Spin operators

The j = 1 spin operators required to form the CGLMP Bell operator (2.25) are given by:

$$S_x = \frac{1}{\sqrt{2}}\begin{bmatrix} 0 & 1 & 0 \\ 1 & 0 & 1 \\ 0 & 1 & 0 \end{bmatrix},\quad S_y = \frac{1}{\sqrt{2}}\begin{bmatrix} 0 & -i & 0 \\ i & 0 & -i \\ 0 & i & 0 \end{bmatrix},\quad S_z = \begin{bmatrix} 1 & 0 & 0 \\ 0 & 0 & 0 \\ 0 & 0 & -1 \end{bmatrix}$$

Appendix 6: Gell-Mann Matrices

The d = 3 Gell-Mann matrices can be viewed as the three-dimensional versions of the Pauli spin matrices and are given by:

$$\lambda_1 = \begin{pmatrix} 0 & 1 & 0 \\ 1 & 0 & 0 \\ 0 & 0 & 0 \end{pmatrix},\quad \lambda_2 = \begin{pmatrix} 0 & -i & 0 \\ i & 0 & 0 \\ 0 & 0 & 0 \end{pmatrix},\quad \lambda_3 = \begin{pmatrix} 1 & 0 & 0 \\ 0 & -1 & 0 \\ 0 & 0 & 0 \end{pmatrix},$$

$$\lambda_4 = \begin{pmatrix} 0 & 0 & 1 \\ 0 & 0 & 0 \\ 1 & 0 & 0 \end{pmatrix},\quad \lambda_5 = \begin{pmatrix} 0 & 0 & -i \\ 0 & 0 & 0 \\ i & 0 & 0 \end{pmatrix},\quad \lambda_6 = \begin{pmatrix} 0 & 0 & 0 \\ 0 & 0 & 1 \\ 0 & 1 & 0 \end{pmatrix},$$

$$\lambda_7 = \begin{pmatrix} 0 & 0 & 0 \\ 0 & 0 & -i \\ 0 & i & 0 \end{pmatrix},\quad \lambda_8 = \frac{1}{\sqrt{3}}\begin{pmatrix} 1 & 0 & 0 \\ 0 & 1 & 0 \\ 0 & 0 & -2 \end{pmatrix},$$

$T_i = \frac{1}{2}\lambda_i$ are generators of SU(3), and thus are used to find the U and V matrices of (2.25) from eight real parameters for each.

Appendix 7: Distribution of sample means of pp→ WZ CGLMP Bell operator expectation value

10^4 sample means, as in Figure 4 for Bell violating processes.

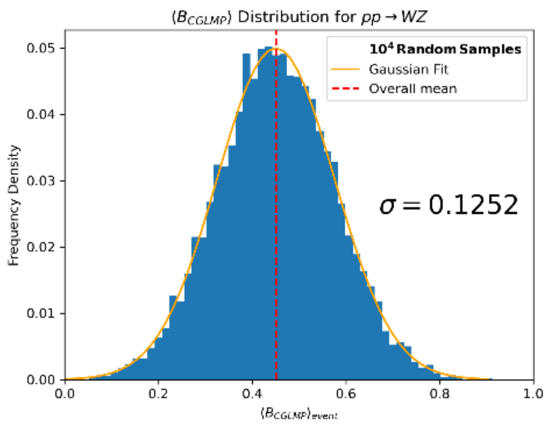

Appendix 8 – Optimised Unitary Transforms

The matrices below correspond to the SU(3) matrices defined in (2.26) to maximise the expectation value of the CGLMP operator for the entire ensemble of 10^6 events.

H → WW:

$$U = \begin{bmatrix} 0.0232558864 - 0.54090673i & 0.433755969 + 0.45820125i & 0.375509612 + 0.40960832i \\ 0.130904485 + 0.53428416i & 0.295584389 - 0.36115381i & 0.116014505 + 0.68274657i \\ -0.521439735 - 0.36384629i & -0.54169158 - 0.30112356i & -0.000447379972 + 0.46001208i \end{bmatrix}$$

$$V = \begin{bmatrix} -0.0012594 - 0.46096468i & 0.54114266 - 0.29905937i & -0.52230614 + 0.36391536i \\ -0.11199192 + 0.6848553i & 0.29519521 + 0.35951386i & -0.1325439 + 0.53335984i \\ 0.37279598 - 0.40861248i & -0.43676227 + 0.45888605i & 0.02114263 + 0.54062398i \end{bmatrix}$$

$H \rightarrow ZZ$:

$$U = \begin{bmatrix} 0.48159721 - 0.23081921i & -0.61972244 - 0.30303627i & 0.34062214 - 0.35053714i \\ 0.68970048 + 0.15879663i & 0.11774759 + 0.01572377i & -0.69435302 - 0.05346991i \\ 0.36848363 - 0.27946969i & 0.63733173 + 0.32219504i & 0.43963799 - 0.28780821i \end{bmatrix}$$

$$V = \begin{bmatrix} 0.45052871 + 0.27866295i & -0.63802052 + 0.32574279i & 0.36218627 + 0.27388576i \\ 0.68920099 - 0.05148247i & 0.12509584 - 0.0172721i & -0.69554212 + 0.15041748i \\ 0.34473416 + 0.35054351i & 0.61899692 - 0.29617052i & 0.48412669 + 0.23027112i \end{bmatrix}$$

Bibliography

[1] J.S. Bell, *On the Einstein Podolsky Rosen paradox, Physics Physique Fizika* **1** (1964) 195.

[2] D.F.V. James, P.G. Kwiat, W.J. Munro and A.G. White, *Measurement of qubits*, *Phys. Rev.* A **64** (2001) 052312.

[3] W. Bernreuther, D. Heisler and Z.-G. Si, *A set of top quark spin correlation and polarization observables for the LHC: Standard model predictions and new physics contributions, Journal of High Energy Physics* **2015** (2015) 1–36.

[4] R. Ashby-Pickering, A.J. Barr and A. Wierzchucka, *Quantum state tomography, entanglement detection and Bell violation prospects in weak decays of massive particle, [arXiv:2209.13990 [quant-ph]].*

[5] M. Fabbrichesi, R. Floreanini, E. Gabrielli and L. Marzola, *Bell inequalities and quantum entanglement in weak gauge bosons production at the LHC and future colliders, [arXiv:2302.00683 [hep-ph]].*

[6] J. Alwall, R. Frederix, S. Frixione, V. Hirschi, F. Maltoni, O. Mattelaer et al., *The automated computation of tree-level and next-to-leading order differential cross sections, and their matching to parton shower simulations, Journal of High Energy Physics* **2014** (2014) .

[7] M. Gell-Mann, *Symmetries of baryons and mesons, Phys. Rev.* **125** (1962) 1067.

[8] F. Li, C. Braun and A. Garg, *The Weyl-Wigner-Moyal formalism for spin, EPL (Europhysics Letters)* **102** (2013) 60006.

[9] G. Barr, R. Devenish, R. Walczak and T. Weidberg, *Particle Physics in the LHC Era, Oxford University Press* 2016 978-0-19-874855-7.

[10] A.J. Barr, *Testing Bell inequalities in Higgs boson decays*, *Physics Letters* B **825** (2022) 136866.

[11] F. Mintert, A. Carvalho, M. Kus and A. Buchleitner, *Measures and dynamics of entangled states, Physics Reports* **415** (2005) 207.

[12] F. Mintert and A. Buchleitner, *Observable entanglement measure for mixed quantum states, Physical Review Letters* **98** (2007).

[13] D. Collins, N. Gisin, N. Linden, S. Massar and S. Popescu, *Bell inequalities for arbitrarily high-dimensional systems*, *Physical Review Letters* **88** (2002).

[14] A. Acin, T. Durt, N. Gisin and J.I. Latorre, *Quantum nonlocality in two three-level systems, Physical Review* A **65** (2002).

[15] Gao, F. and Han, L. *Implementing the Nelder-Mead simplex algorithm with adaptive parameters*. Computational Optimization and Applications. **51:1** (2012), pp. 259-277.

Other resources potentially contributing:

B. R. Martin, G.Shaw *Particle Physics*, *Wiley*, 2008.

D . H. Perkins, *Introduction to High Energy* Physics, Cambridge University Press 2000.